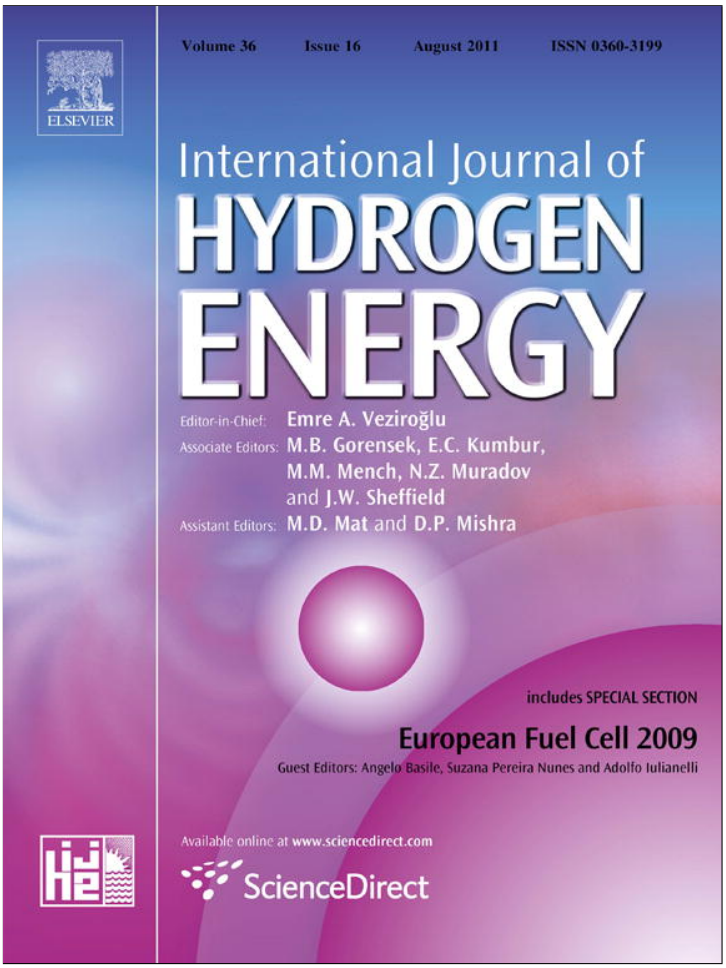

INTERNATIONAL JOURNAL OF HYDROGEN ENERGY 36 (2011) 9405–9414

Available at www.sciencedirect.com

ScienceDirect

journal homepage: www.elsevier.com/locate/he

Preparation and characterization of Co–Ru/TiO_2/MWCNTs electrocatalysts in PEM hydrogen electrolyzer

Perica Paunović [a,*], *Dafinka Stoevska Gogovska* [a], *Orce Popovski* [b], *Antonia Stoyanova* [c], *Evelina Slavcheva* [c], *Elefteria Lefterova* [c], *Peter Iliev* [c], *Aleksandar T. Dimitrov* [a], *Svetomir Hadži Jordanov* [a]

[a] *Faculty of Technology and Metallurgy, University "Sts. Cyril and Methodius", Ruger Bošković Str., 16, 1000 Skopje, Macedonia*
[b] *Military Academy, Mihajlo Apostolski Str., b.b., 1000 Skopje, Macedonia*
[c] *Institute of Electrochemistry and Energy Systems, Bulgarian Academy of Sciences, Acad. G. Bonchev Str., Bl. 11, 1113 Sofia, Bulgaria*

ARTICLE INFO

Article history:
Received 2 February 2011
Received in revised form
25 March 2011
Accepted 3 April 2011
Available online 22 June 2011

Keywords:
Hyper–hypo d-electrocatalysts
Water electrolysis
Co
Ru
Anatase
MWCNTs

ABSTRACT

The subject of this study is preparation and characterization of hypo–hyper d-electrocatalysts with reduced amount of precious metals aimed for water electrolysis. The studied electrocatalysts contain 10% mixed metallic phase (Co:Ru = 1:1 wt., Co:Ru = 4:1 wt. and Co:Ru:Pt = 4:0.5:0.5 wt.), 18% TiO_2 as a crystalline anatase deposited on multiwalled carbon nanotubes (MWCNTs). Previously, MWCNTs were activated in 28% nitric acid. As a reference electrocatalyst for hydrogen evolution reaction, corresponding electrocatalysts with pure Pt metallic phase and mixed CoPt (Co:Pt = 1:1 wt.) metallic phase were prepared. Also, as a reference electrocatalyst for oxygen evolution reaction, electrocatalyst with pure Ru metallic phase was prepared.

The prepared electrocatalysts were structurally characterized by means of XPS, XRD, TEM, SEM and FTIR analysis.

Electrochemical characterization was performed by means of cyclic voltammetry and potentiodynamic method in the PEM hydrogen electrolyzer. The range of the catalytic activity for hydrogen evolution of studied electrocatalysts was the following: CoRuPt (4:0.5:0.5) > CoPt (1:1) > Pt > CoRu (1:1) > CoRu (4:1). The order of the catalytic activity for oxygen evolution was the following: CoRu (1:1) > Ru > CoRu (4:1) > Pt > CoRuPt (4:0.5:0.5) > CoPt (1:1).

1. Introduction

One of the most important issues of the hydrogen economy is the choice of the electrode materials for hydrogen evolution/oxidation and oxygen evolution/reduction in hydrogen electrolyzers/fuel cells. The electrode materials are the crucial part of the Membrane Electrode Assembly (MEA) – the driving force of the fuel cells and hydrogen electrolyzers. The power efficiency of MEA depends on the material characteristics of both the electrodes (electronic conductors) and membranes (ionic conductors) as well as on the architecture of the triple phase boundary [1–5].

The natural choice of electrode material for hydrogen evolution reaction is Pt [6]. But, due to the high price and limited resources, the application of Pt in the future will be limited [7]. It is similar with the most active electrode material

* *Corresponding author.*
E-mail address: pericap@tmf.ukim.edu.mk (P. Paunović).
0360-3199/$ – see front matter
doi:10.1016/j.ijhydene.2011.04.014

for oxygen evolution – Ru or more exactly RuO_2 [8]. So, the tendency of the modern electrocatalysis is to reduce or completely replace precious metals in the MEA, keeping the same level of efficiency. There are two approaches to overcome this problem. The first one is mixing of non-precious metals with dissimilar electronic character gaining pronounced synergetic effect of electrocatalytic activity (ex., Jakšić hypo–hyper d-concept [9–11]). The hypo and hyper d-component may be in metallic or in valence state, so there are many combinations of hypo–hyper d-electrocatalysts. Paunović has distinguished these catalysts in 5 main groups [12]: i) intermetallic catalysts, ii) metal-sulfides/phosphides, iii) catalysts based on Raney Ni, mixed oxides and v) hypo oxide – hyper metal. Nanostructured catalysts require much stronger bonding supports, for both long-term stability and higher activity through hypo–hyper d-interaction. In this respect titania has an unique role [11]. This role of TiO_2 was emphasized by Tauster in heterogeneous catalysis [13]. The second approach is replacement of the traditional support material – carbon blacks with carbon nanotubes CNTs [14–17]. CNTs show superior characteristics related to the carbon blacks. Also, they have considerably higher electronic conductivity of 10^4 S cm^{-1} [7] than that of Vulcan XC-72, 4.0 S cm^{-1}, while specific surface area is in range of 200 ÷ 900 m^2 g^{-1} [14] vs. Vulcan XC-72 of 250 m^2 g^{-1}. Other advantage of CNTs vs. Vulcan XC-72 is higher chemical, i.e. corrosion stability [18].

The previous papers of the present authors were concerned with hypo–hyper d-electrocatalysts based on non-platinum metals (Me/TiO_2/MWCNTs, Me = Ni, Co, CoNi) [19–21]. Co-based electrocatalysts have shown the best performances in alkaline electrolyzers. The activation of MWCNTs by nitric acid improves the performances of the Co-based electrocatalyst [17]. But, the catalytic activity of Co and Ni-base systems in proton exchange membrane (PEM) electrolyzer was poor due to their instability in acid media [22]. So, the further research was oriented to electrocatalysts with mixed metallic phase containing Co and Pt [23]. Co has been shown as a promoter of reducing Pt particles. So, electrocatalyst with only 20% Pt wt. in metallic phase has shown close activity to that with pure Pt metallic phase, while the activity of electrocatalyst with 50% Pt wt., is considerably higher than that of pure Pt-based electrocatalyst.

The aim of this paper is to study electrocatalytic activity of hypo–hyper d-electrocatalysts containing mixed Co–Ru metallic phase deposited on activated MWCNTs and TiO_2 anatase in PEM hydrogen electrolyzer. For comparison corresponding electrocatalyst with pure Pt and mixed CoPt metallic phase were prepared.

2. Experimental

The common composition of the studied electrocatalysts is 10% wt. metallic phase (CoRu, CoPt and Pt, see Table 1), 18% wt. TiO_2 and the rest – multiwalled carbon nanotubes (MWCNTs) as a carbon substrate. Me-2,4-pentanedionate, Me = Co, Ru or Pt, Alfa Aesar, Johnson Matthey, GmbH was used as precursor for metallic phases, while Ti-isopropoxide, Aldrich, 97% was used as precursor for TiO_2. Metallic phases and TiO_2 were grafted over the carbon substrate by sol–gel procedure. As a carbon substrate MWCNTs (*Guangzhou Yorkpoint Energy Company, China*) were used. Previously they were treated in 28% wt. nitric acid at room temperature for 4 h [17]. In the first stage, in order to deposit (TiO_2) onto carbon substrate, Ti-isopropoxide (Aldrich, 97%) was added into dispersed activated MWCNTs in anhydrous ethanol. To provide hydrolysis to $Ti(OH)_4$, small amount of 1 M HNO_3 was added. This mixture was evaporated at 60 °C with continuous intensive stirring until fine nano-structured powder of catalyst support was obtained. Further, individual or mixed Me-2,4-pentaedionate was dissolved in anhydrous ethanol. This solution was added into dispersed catalyst support in anhydrous ethanol. The evaporation was carried out under the same conditions as above. The aim of this operation is to graft the metal-hyper d-phase onto catalyst support. To decompose both $Ti(OH)_4$ to TiO_2 and the residual amount of oraganometallics, the powder was heated for 2 h at 480 °C in the atmosphere of $H_2 + N_2$.

Table 1 – Composition of the studied electrocatalysts.

Sample no	Hyper-metal d-phase (10%)	Hypo-oxide d-phase (18%)	Carbon substrate (72%)
1	CoRu (1:1, wt.)	TiO_2	MWCNTs
2	CoRu (4:1, wt.)	TiO_2	MWCNTs
3	CoRuPt (4:0.5:0.5, wt.)	TiO_2	MWCNTs
4[a]	Ru	TiO_2	MWCNTs
5[b]	Pt	TiO_2	MWCNTs
6[b]	CoPt (1:1, wt.)	TiO_2	MWCNTs

a Sample 4 containing pure Ru metallic phase was prepared as a reference material for oxygen evolution reaction.
b Samples 5 and 6 were used as a reference material for hydrogen evolution reaction. Their structural characteristics are shown in our previous paper [23].

The prepared electrocatalysts of general composition Me–TiO_2-MWCNTs are summarized in Table 1.

To identify the intrinsic changes caused by the change of the electrocatalysts composition, spectroscopic and structural techniques were employed such as XRD, SEM, TEM, XPS and FTIR. XRD measurements were carried out by X-Ray diffractometer Philips APD 15, with CuK_α radiation. The X-ray diffraction data were collected with at a constant rate of 0.02° s^{-1} over an angle range of 2θ = 10–90°. Microscopic observation of the studied electrocatalysts was performed by Transmission Electron Microscope JEOL, model JEM 200 CX, used in scanning (SEM analysis) and transmission regime (TEM analysis). Infrared spectroscopy was employed to determine the strength of hypo–hyper d-interaction (TiO_2/Me), using FTIR spectrometer model Bruker Vector 22. XPS analysis was performed using ESCALAB MK II (VG Scientific, England) electron spectrometer. The photoelectrons were excited with a twin anode X-ray source using Mg–Kα ($h\nu$ = 1253.6 eV) radiation. C1s photoelectron line at 284.50 eV was used as a reference for calibration. The XPS peaks obtained were deconvoluted and fitted with the freeware FITT program (version 1.2,) [24].

The performances for hydrogen/oxygen evolution reaction of the prepared electrocatalysts were tested into PEM

hydrogen electrolyzers. The design of the PEM electrolyzer and its operational principle is described elsewhere [25]. The MEAs contain working electrode of the studied electrocatalysts and counter electrode of the Pt E-Tek containing 30% Pt, both grafted on a commercial Nafion 117 membrane (Alfa Aesar). The presented electrode potentials were measured versus RHE (a small piece of Pt E-Tek containing 30% Pt, ca. 0.1 cm^2) at the given testing conditions. All electrochemical measurements in PEM electrolyzer were carried out by Galvanostat/Potentiosat POS 2, Bank Electronik, and CPCDA software.

The MEAs have a complex multilayer structure consisting of gas diffusion, backing, and catalytic layers. The backing layer was made of a mixture of carbon particles (Shawinigan Acetylene Black) and 30% of PTFE suspension, deposited on thin carbon cloth, serving as a gas diffusion layer. The catalytic layer was spread upon the backing one as an ink (catalyst particles mixed with diluted Nafion ionomer) by several steps. After each step the electrode was dried for 30 min at 80 °C and weighed using an analytical microbalance Boeco, Germany. The procedure was repeated until a metallic phase loading of 0.5 mg cm^{-2} was reached. Then the electrodes were hot pressed onto the PEM electrolyte forming the test MEA. The hot pressing was performed stepwise in the regime of gradual temperature and pressure increase starting from 50 °C to 6 kg cm^{-2} and ending with 120 °C and 12 kg cm^{-2}, respectively.

3. Results and discussions

3.1. XRD analysis

Identification of the present phases in the studied electrocatalysts was performed by XRD analysis. XRD spectra are shown in Fig. 1. In all samples, characteristic peaks for TiO_2 with anatase crystalline structure were detected. It was estimated that the size of anatase particles is 5 nm. For values of 2θ of 25,46°; 43,21° and 57,2°, characteristic peaks for graphite were detected, originated by the carbonaceous support material – MWCNTs.

The presence of characteristic peaks of Ru, Co or Pt was not detected. This can be result of both their very small particle size (<2 nm) as well as of the amorphous character of their oxides. The amorphous character of Co in the corresponding electrocatalysts produced by the same procedure, and its particles of 2 nm were detected in the previous works of the present authors [20–22]. As the contribution of Co increases to 80% in the metallic phase (samples 1 and 2), inception of the peak characteristic for crystalline Co was detected at 2θ = 44,3°. For sample 3 (with CoRuPt metallic phase Co:Ru:Pt = 4:0.5:0.5 wt.) new peaks at 2θ = 31,24°; 36,55°; 43,78°; 59,35° appear. These peaks correspond to Co_3O_4.

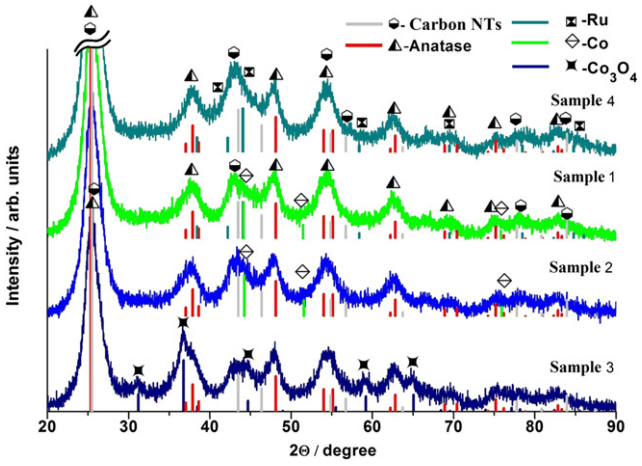

Fig. 1 – XRD spectra of the studied electrocatalysts.

In sample 3 diffraction lines of fcc Pt (only 10% Pt) is not detected. Our supposition is that Pt is present in oxidized form. In our previous work, it was found that Pt particles in presence of Co showed considerably reduced size [23]. In the electrocatalyst with pure Pt as metallic phase, particle size of Pt were 12 nm, while in the electrocatalyst with mixed metallic phase CoPt (Co:Pt = 4:1, 1:1 wt.), they were reduced to 3 ÷ 4 nm.

3.2. TEM and SEM analysis

To observe catalyst's particles and morphology, TEM and SEM analysis was done (Fig. 2). In all catalysts size of the particles is mainly lower than 5 nm. As the contribution of Co in the metallic phase increases (sample 2 and 3 with 80% Co) larger

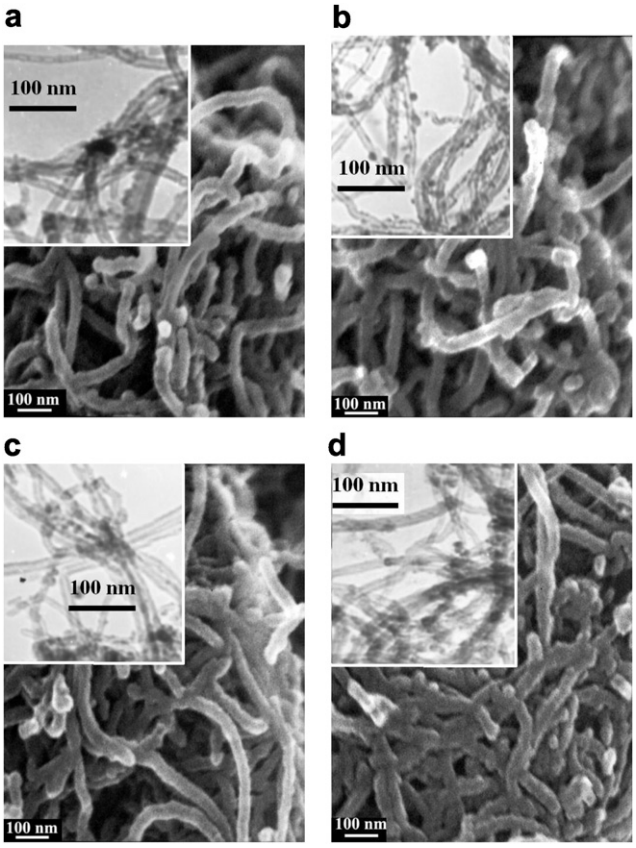

Fig. 2 – SEM and TEM images: a) sample 1–10% CoRu (1:1 wt.) + 18% TiO_2 + MWCNTs; b) sample 2–10% CoRu (4:1 wt.) + 18% TiO_2 + MWCNTs; c) sample 3–10% CoRuPt (4:0.5:0.5 wt.) + 18% TiO_2 + MWCNTs; d) sample 4–10% Ru + 18% TiO_2 + MWCNTs.

particles appear ~10 nm. This is the result of presence of crystalline Co which was detected by XRD analysis. The diameter of the MWCNTs is ~15 nm.

According to SEM images, the studied electrocatalysts have intertwined thread-like morphology, as a result of presence of the MWCNTs. This morphology is more appropriate than that of electrocatalysts deposited on Vulcan XC-72 [19,20]. Here, the catalyst's components are grouped into smaller clusters. Also, there are more holes between them which lead to better inter-particle porosity of the catalyst. Due to the intrinsic geometric shape of MWCNTs, empty cylinders ordered one over the other, they possess inner holes, so the inner or trans-particle porosity of electrocatalysts deposited on MWCNTs is considerably higher.

3.3. *XPS analysis*

In order to complete the statement and to explain some unclearness of the XRD analysis, XPS analysis was performed. Also, this analysis is appropriate to verify strong metal-support interaction (SMSI) through the hypo–hyper d-interaction between metallic phase (hyper d-phase) and catalyst support (containing TiO_2 as hypo d-phase), as the main promoter of improved catalytic activity of the hypo–hyper d-electrocatalysts.

The determination of the different Ru valence states complicates from the overlapping between Ru 3d doublet with the strong C1s peak (Fig. 3) and $Ru3p_{3/2}$ with Ti2p peaks (Fig. 4). Shown in Fig. 3 are the C1s-Ru3d core-level spectra of the studied electrocatalysts. The C1s spectra are typical for carbon nanotubes with the characteristic asymmetry on the high energy side and are deconvolured into six component. The main component, situated at 284.5 eV corresponds to sp^2 hybridized (3-fold) graphite-like carbon double bonding (C=C). The peak at 285–285.5 eV is related to some structural defects at the surface of the graphitic sheet as the single bonding carbons (C–C) and sp^3 hybrid orbital. The concentration of surface defects is increased as result of the shortening and opening of the MWCNTs during purification/activation process in HNO_3. The peaks around 286.4, 287.8, 289 and 291 eV (see Fig. 2) correspond to C–O, C=O (or/and C–OH), –O–C=O (COO) bonds and the $\pi \rightarrow \pi^*$ shake-up, respectively [26–28]. There are no significant changes in the C1s spectra of the different catalysts.

The distinct additional peak at the low energy side (280–283 eV) for catalyst 4 is assigned to Ru3d photoemission This peak can deconvolute into three doublets corresponding to Ru(0) (280.2–280.5 eV), Ru(IV) (~281.3 eV) and Ru(VI) (~282.5 eV) (see Fig. 3b). According to literature, the binding energy of metallic Ru is 280.2 eV [29,30]. In our case it is slightly higher (280.45 eV). This may due to hypo–hyper interaction between Ru and TiO_2, by analogy with hypo–hyper interaction between Pt and TiO_2 [11] as well as to the small size effect. The intensity of the component Ru(0) drastically decreases with Co

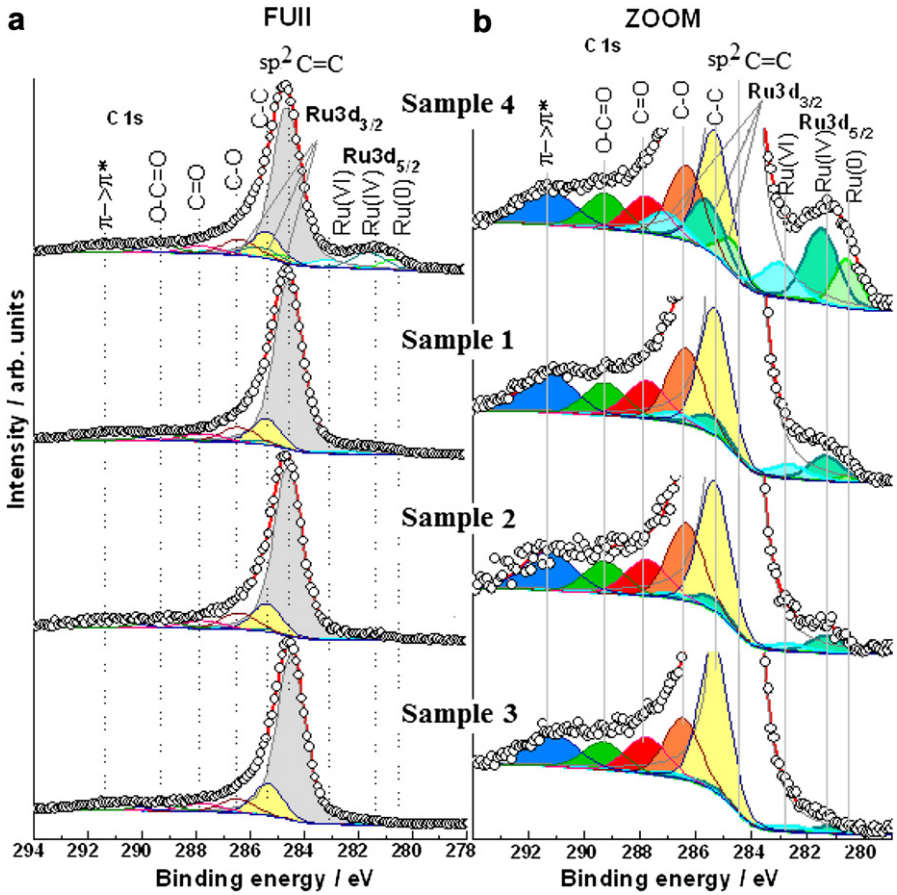

Fig. 3 – C1s-Ru3d core-level photoelectron spectra of the studied electrocatalysts: a) full spectra, b) zoomed spectra.

addition and it disappears in the Ru3d spectra for sample 2 and 3 (Co:Ru = 4:1 and Co:Ru = 4:0,5 wt., respectively).

Additional information about Ru is given in the Fig. 4, where at Ti2p and $Ru3p_{3/2}$ core-level spectra are shown. The XPS spectrum of the sample 4 (electrocatalyst with pure Ru) initially was deconvoluted into four components. The Ti2p doublet at ~459 eV corresponds to TiO_2. The rest three single peaks are assigned to Ru3p3/2 core-level spectra of the ruthenium in three different valence states: Ru(0) (~462 eV), Ru(IV) (~463.5 eV) and Ru (VI) (465.5 eV). For sample 1, the position of Ru(0) is almost the same as in the sample 4, therefore Ru3p3/2 spectra of the samples 1 and 4 are in well correlation with the Ru3d spectra. For samples 2 and 3 (with increased quantity of Co), this component of the spectra is shifted to lower binding energies for ~1 eV., i.e. at ~460.5 eV. Taking account the results from Ru3d this component cannot connect with the Ru(0) and hence belongs to the Ti2p core-level spectra. That's why it is included additionally in the deconvolution of the all spectra (component * in Fig. 4). The higher binding energy compared to the main Ti2p3/2 peak can be explained with the interaction between hypo Ti and hyper Ru, Co and Pt components as well as to formation of mixed oxides such as RuO_2–TiO_2 and CoO–TiO_2 [30–32].

Shown in Fig. 5 are Co2p core-level spectra. The $Co2p_{3/2}$ binding energies of Co(II) and Co(III) species are close. However, the $Co2p_{3/2}$–$Co2p_{1/2}$ separation and satellite structure are useful in characterization of the cobalt chemical environment. The $Co2p_{3/2}$–$Co2p_{1/2}$ separation is ~16 eV for Co(II) and 15 eV for Co(III) and Co(0). As result, the $Co2p_{1/2}$ peak exhibits a high differences between of Co(II) and Co(III) species [33,34,35]. In the high spin compounds such as CoO, Co(II) ions are situated in the octahedral sites in the rock-salt-like structure and exhibit strong satellite lines which are located at ~5–6 eV above the main line. In the low spin compounds such as Co_3O_4, Co(III) ions are in octahedral sites, while Co(II) in tetrahedral sites as spinel-like structure and Co2p spectra exhibits a weak satellite shifted by 10 eV to higher binding energies. The spectrum of metallic cobalt Co(0) (778 eV) does not contain shake-up satellite [32,33,36]. Taking into account the above-mentioned, the Co 2p spectra were deconvoluted into three spin-orbit doublets, corresponding to at ~778 eV, Co(II) at ~781 eV and Co(III) at ~780 eV and two satellites Sat.(II) at ~787 eV and Sat(III) at ~791 eV. The spin-orbital splitting is 15–15.2 eV for Co(0) and Co(III) species and 15.7–16 eV for Co(II) species.

For sample 1 with mixed metallic phase CoRu (Co:Ru = 1:1 wt.), $Co2p_{3/2}$ peak at position of 781.2 eV (high spin-orbital splitting at 15.7 eV) and the strong satellite at 786.5–787 eV show that Co exists in second valence state, most probably as $Co(OH)_2$ (~781.3 eV). Small amount of Co(0) exists too. On the spectra of samples 2 and 3 (with 80% Co), the widening of the $Co2p_{1/2}$ peak toward lower binding energy connects with the presence of Co(III). It is in correlation with the satellite component at ~791 eV and with the availability of

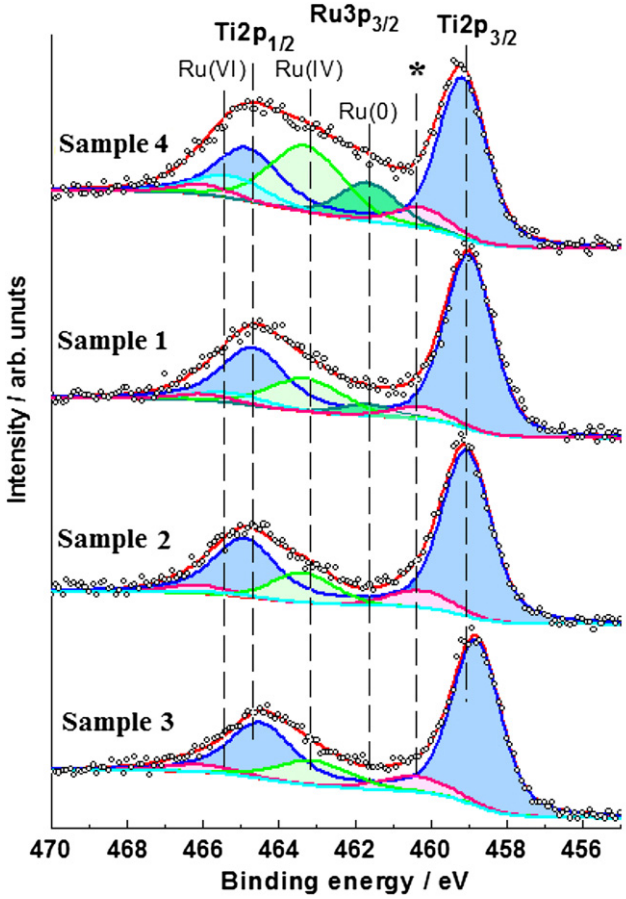

Fig. 4 – Ti2p and Ru3p core-level spectra.

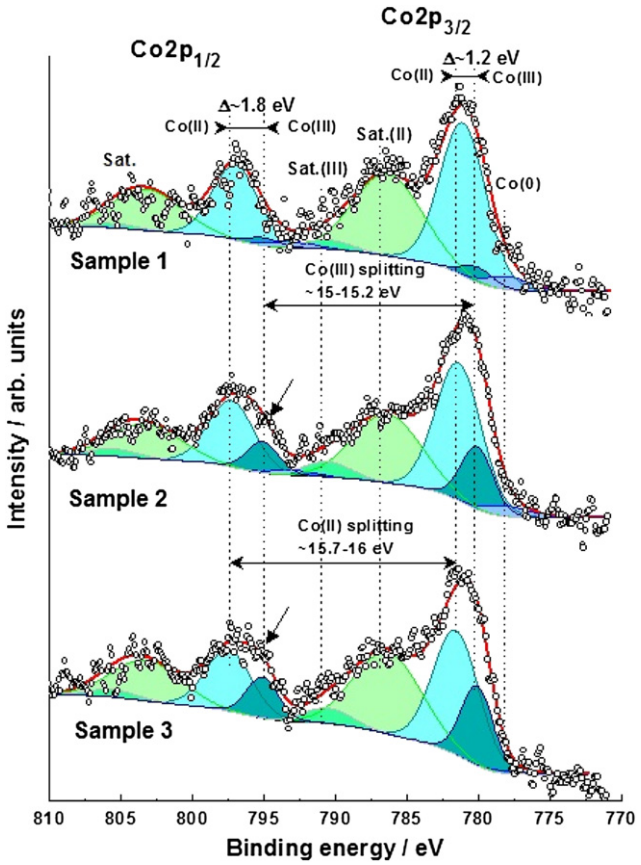

Fig. 5 – Co2p core-level photoelectron spectra.

Co_3O_4, established from XRD. This means that Co (II) component is a superposition of Co in two different positions – Co(II) in octahedral sites, which is dominant and Co(II) in the tetrahedral sites in the spinel-like structure. This can explain the slight shift to higher binding energies from 781.2 to 781.7 eV.

Shown in Fig. 6 is 4f XPS spectrum originated by sample 3 (containing 10% Pt). This spectrum was deconvoluted into 3 doublets corresponding to Pt(0) ~71.2 eV, Pt(II) ~72.5 eV and Pt(IV) ~75.0 eV. As it can be seen, platinum presents in oxidized form which is in accordance with the XRD results. The binding energy at ~72.5 eV correspond to $Pt(OH)_2$, while the component at 75 eV to PtO_2. The formation of mixed Pt–O–Me (Me = Ti, Co, Ru) bonds is not excluded.

The asymmetric and broad O1s peak (Fig. 7) is due to different oxygen bonds and environment. O1s peak is deconvoluted into three components. The main component situated at lower binding energy (about 529–530 eV) is due to the oxygen in the Me–O bonds in MeOx (Me = Ru, Co, Pt, Ti) as well as to C=O bond. The O1s component around 531.5–532 eV corresponds to Me–OH and C–O bonds.

According to O1s, Co2p and Pt4f XPS core-level spectra, one can conclude that a part of Co(II) and Pt(II) states exist as hydroxide form, i.e. as $Co(OH)_2$ and $Pt(OH)_2$. The high energy component (533.5–534 eV) can be assigned to adsorbed H_2O and/or –C=O bonds [37,38].

3.4. *FTIR analysis*

According to Jakšić's hypo–hyper d-theory for electrocatalysts, as result of interaction between hypo and hyper d-components, i.e. TiO_2 and metallic phase (Co, CoRu, CoRuPt or Ru) the intrinsic catalytic activity increases. The intensity of this hypo–hyper d-interaction can be determined by infrared spectroscopy. Shown in Fig. 3a are the FTIR spectra of the studied electrocatalysts. The only band of interest within the

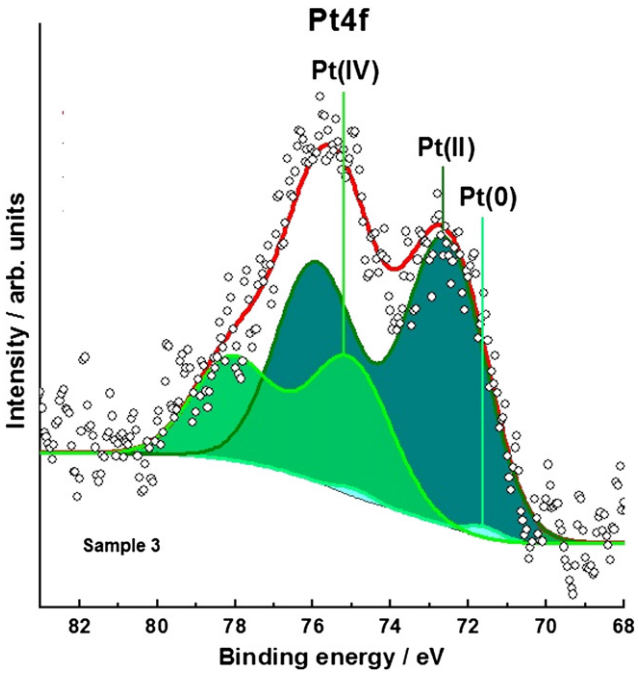

Fig. 6 – Pt4f core-level spectrum of the sample 3.

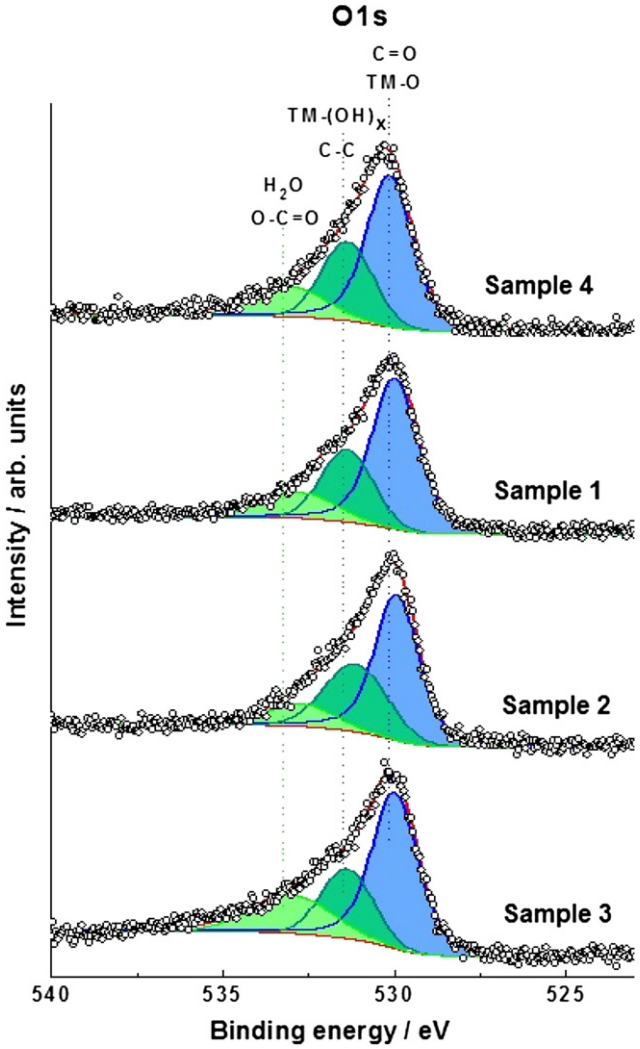

Fig. 7 – O1s deconvoluted photoelectron spectra.

spectra originates by TiO_2 [19,23]. In the Fig. 8 the region of FTIR spectra where TiO_2 band exists is shown for each sample. To determine hypo–hyper d-interaction one has to compare TiO_2 band from each electrocatalyst and the band from pure TiO_2 obtained in identical conditions. The maximum of the band of pure TiO_2 is located at wave number value of 495 cm^{-1} [23]. The maximum of TiO_2 bands from the electrocatalysts is shifted at higher values of wave number. The higher the shift of the wave number, the shorter the bond between the TiO_2 and the hyper d-metallic phase, i.e. the higher the hypo–hyper d-interaction. All investigated samples show almost the same shift of the wave number value of bands maximum, ~905 cm^{-1}. This means that the intensity of hypo–hyper d-interaction in all samples is the same. Therefore, in all samples there is an increase of the intrinsic catalytic activity and this rise is equal for all studied electrocatalysts.

3.5. *Cyclic voltammetry*

Cyclic voltammograms performed in the whole potential range between hydrogen and oxygen evolution (Fig. 9) give qualitative informations about the nature of the processes

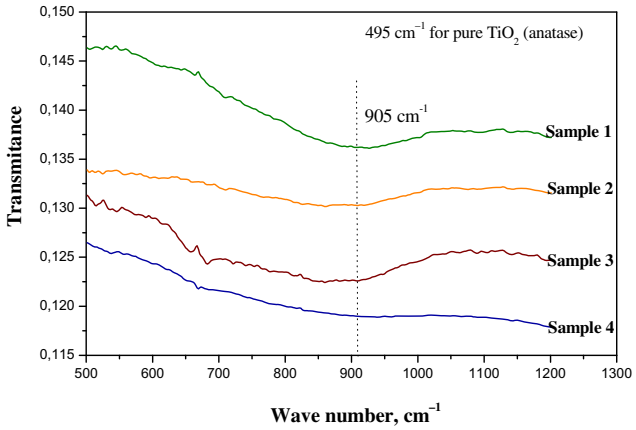

Fig. 8 – FTIR spectra of the studied electrocatalysts.

occurring on the catalyst surface. The measurements were performed at room temperature with scanning rate of 100 mV s^{-1}. The potential is expressed vs. reference hydrogen electrode (RHE). In the Fig. 9a, voltammogram for hypo–hyper d-electrocatalysts with pure metallic phase (Ru and Pt) are shown. These samples were chosen as reference ones for

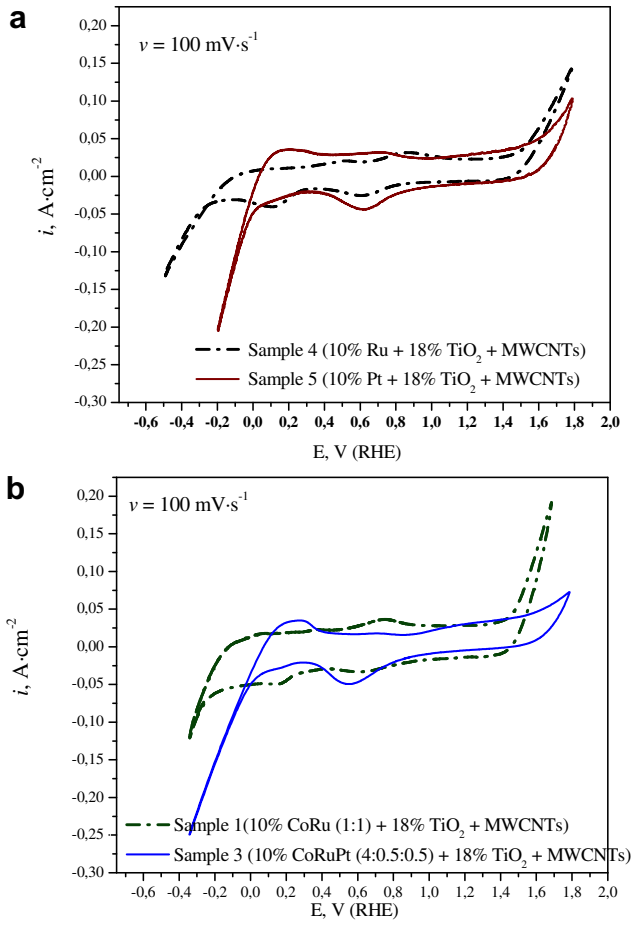

Fig. 9 – Cyclic voltammograms of the studied electrocatalysts at room temperature and scan rate of 100 mV s^{-1}.

oxygen and hydrogen evolution reaction, respectively. Both voltammograms contain corresponding peaks characteristic for transition of the metallic phase to the higher valence state, i.e. formation of the oxygen coverage (Me–O, Me–OH). For Ru-based catalysts there are two peaks of this type at 0.52 and 0.85 V. They represent transition to Ru(IV) at 0.52 V and to Ru(VI) at 0.85 V. Corresponding opposite peaks registered during opposite potential scan were registered 0,62 and 0.12 V, respectively. For Pt-based catalyst peaks corresponding to the hydrogen adsorption/desorption processes are situated in the potential range between 0.12 and 0.35 V. The peak characteristic for oxygen coverage at ~0.78 V is stretched and not well shaped. The opposite peak is well shaped and was registered at 0.62 V. Hydrogen evolution reaction (HER) on the Pt-based electrode is considerably more intensive and starts at lower potential for ~0.22 V related to the Ru-based electrode. Oxygen evolution reaction (OER) occurs more intensively on the Ru-based electrode and starts at lower potentials for 0.12 V. So, Pt-based electrocatalyst is better for HER, while Ru-based one is better for OER.

Cyclic voltammograms of the studied electrocatalysts are shown in Fig. 9b. Sample 1 with mixed CoRu metallic phase (Co:Ru = 1:1 wt.) shows similar voltammogram as Ru-based catalyst shown in Fig. 9a. In this case, due to overlapping of more surface processes occurring over the Ru and Co surface some characteristic peaks have anomalous shape or disappeared. Its asymmetric shape is result of heterogeneous forming of $Co(OH)_2$ and CoO into so called sandwich-structure $Co/CoO/Co(OH)_2$ during Co(0) to Co(II) transformation [39] and a sandwich-structure $CoO/Co(OH)_2/Co_3O_4$ during Co(II) to Co(III) transformation [40]. These sandwich-structures are very suitable for further easier oxygen evolution. Sample 2 with mixed CoRu metallic phase (Co:Ru = 4:1 wt.) has shown similar voltammogram with less intensive electrode reactions (HER and OER), but for clear presentation of the results, this voltammogram was not shown. The voltammogram of the sample 3 (mixed metallic phase Co:Ru:Pt = 4:0.5:0.5 wt.) is very similar to that of Pt-based electrocatalyst, although the amount of Pt in the electrocatalyst is very low. HER on this catalyst starts at lower potential for 0.2 V related to the sample 1, while OER starts at higher potential for 0.13 V. Sample 1 behaves as Ru-based electrocatalyst, while sample 3 as Pt-based one.

3.6. *Electrocatalytic activity for HER*

Polarization curves for HER shown in Fig. 10 were obtained by potentiodynamic method with scan rate of 2 mV s^{-1} at room temperature. Samples 5 and 6 containing CoPt (1:1 wt.) and pure Pt as metallic phase (studied in our previous paper [23]) were chosen as reference materials to estimate electrocatalytic activity for HER of the studied CoRu-based electrocatalysts.

The order of the catalytic activity for hydrogen evolution of the studied hypo–hyper d-electrocatalysts with general composition 10% Me + 18% TiO_2 + MWCNTs is the following: CoRuPt (4:0.5:0.5) > CoPt (1:1) > Pt > CoRu (1:1) > CoRu (4:1). One should consider that all electrocatalyst are deposited on the same carbon support – activated MWCNTs with TiO_2 – anatase with the same size of particles. XPS analysis has shown the presence of strong metal-support through the

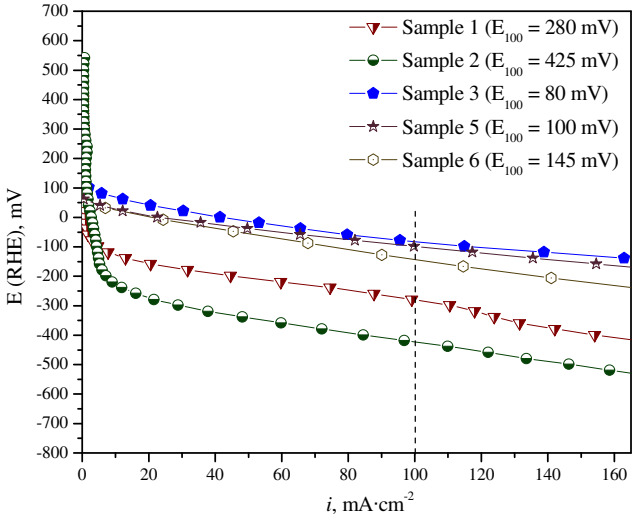

Fig. 10 – Galvanostatic polarization curves of the studied electrocatalysts for HER at 20 °C.

hypo–hyper d-interaction between TiO_2 and metallic phase, i.e. through the presence of mixed hypo–hyper d-compounds such as RuO_2–TiO_2, CoO–TiO_2 etc. FTIR analysis has shown the same level of hypo–hyper d-interaction between metallic phases and TiO_2, thus the rise of the intrinsic activity of all studied electrocatalysts is the same. Also, according to the XRD characterization, all metallic components have the similar size of particles. Therefore, the difference in electrocatalytic activity is result of the intrinsic activity of the catalytic metallic phase into the studied samples.

So, sample 3 with very low amount of Pt into the metallic phase shows superior catalytic activity for HER compared with the other studied CoRu-based electrocatalysts. Also, this catalyst shows better activity than corresponding Pt (sample 5) and CoPt-based (sample 6) catalyst having 10 and 5 times higher content of Pt respectively. Comparing the catalytic activity of the Pt-containing catalysts one can notice paradoxal order of activity, i.e. catalytic activity for HER increases as the Pt content in the samples decreases. In our previous paper [23], it was shown that Co behaves as promoter for reduction of Pt particle size. So, the size of Pt particles in electrocatalyst with pure Pt metallic phase was 12 nm, while in the presence of Co (Co:Pt = 1:1 wt.), the size was reduced to 4 nm. The catalytic activity of the CoPt catalyst was higher. The lower amount of Pt was compensated by the highly developed surface of Pt-phase in the mixed systems. In this study, the ratio of Co:Pt is higher (8:1 wt.) and the size of Pt particles reaches ~2 nm. The surface area of Pt particles (the active catalytic centers) in this case is more developed contributing to higher catalytic activity.

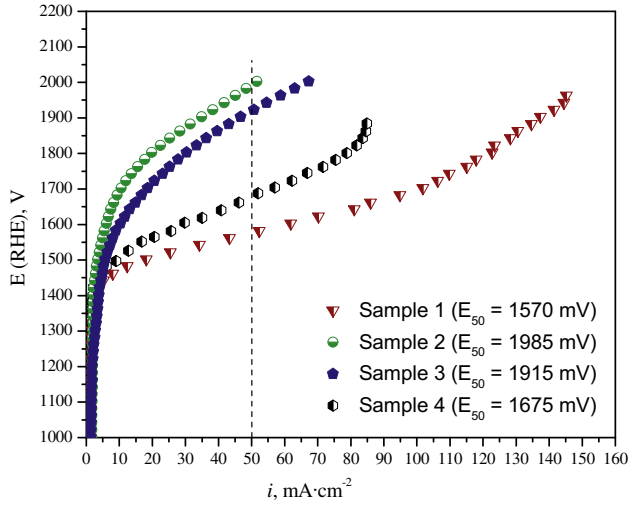

Fig. 11 – Galvanostatic polarization curves of the studied electrocatalysts for OER at 20 °C.

3.7. *Electrocatalytic activity for OER*

Polarization curves for OER obtained in the same conditions as for HER are shown in Fig. 11. As a reference material for estimation of catalytic activity for OER of the studied samples, Ru-based electrocatalyst was chosen (sample 4).

The order of catalytic activity of the catalysts with general composition 10% Me + 18% TiO_2 + MWCNTs for OER is the following: CoRu (1:1) > Ru > CoRuPt (4:0.5:0.5) > CoRu (4:1). Electrocatalyst with CoRu (1:1) metallic phase has shown the best catalytic activity, even better than the reference one containing pure Ru as metallic phase. It is well known that the surface structure of the electrode in the solution is the feature that distinguishes the oxide electrodes [41,42]. Their surface is with high energy content and with strong hydrophilic character, so that it attracts water molecules and gives a layer of OH groups on top of the oxide. This layer mediates the action of the oxide's surface with the solution species. The OH groups are responsible for the exhibited electrocatalytic activity. In this context, the presence of Co in the metallic phase, i.e. surface sandwich-structure of Co oxides and hydroxides (CoO/$Co(OH)_2$/Co_3O_4) is very suitable for oxygen evolution. On the other side, the presence of hypo–hyper d-mixed oxides CoO–TiO_2, RuO_2–TiO_2 on the surface is also suitable for OER.

With further increase of the Co content in the metallic phase, i.e. decrease of the Ru content (samples 2 and 3) catalytic activity for OER decreases. So, the optimal ratio of Co and Ru in the metallic phase is 1:1 wt.

4. Conclusions

The main goal of this study was to produce nano-scaled electrode materials with reduced load of precious metals in self-developed electrocatalysts for HER and OER. Metallic phase (Co, Ru and Pt) was deposited on catalyst support consisted of MWCNTs activated in HNO_3 and anatase titania with particle size of 4 nm as promoter of hypo–hyper d-interaction. According to the above results the follow conclusions can be drawn:

1. The presented synthesis method provide production of nano-scaled catalytic materials with very small particles (~2 nm) of the metallic active catalytic centers and pronounced strong metal-support interaction (SMSI) through the hypo–hyper d-interaction between hyper d-metallic phase and hypo d-oxide phase TiO_2. The level of hypo–hyper

d-interaction between metallic phase and TiO_2 was the same for all studied electrocatalysts.

2. Electrocatalyst containing CoRuPt (4:0.5:0.5 wt.) has shown the best catalytic activity for HER compared with the other CoRu and CoPt-based electrocatalysts. The lower amount of Pt was compensated by the highly developed surface of Pt-phase in the mixed systems as result of very small particles of Pt.
3. Electrocatalyst containing CoRu (1:1 wt.) has shown the best catalytic activity for OER. The presence of mixed hypo–hyper d-oxides on the catalyst's surface ($CoO–TiO_2$, $RuO_2–TiO_2$) contribute to increased catalytic activity related to the electrocatalyst containing pure Ru as metallic phase.

REFERENCES

[1] Yoon YG, Park GG, Yang TH, Han JN, Lee WY, Kim CS. Effect of pore structure of catalyst layer in a PEMFC on its performance. Int J Hydrogen Energy 2003;28(6):657–62.

[2] Smirnova A, Dong X, Hara H, Vasiliev A, Sammes N. Novel carbon aerogel-supported catalysts for PEM fuel cell application. Int J Hydrogen Energy 2005;30(2):149–58.

[3] Radev I, Slavcheva E, Budevski E. Investigation of nanostructured platinum based membrane electrode assemblies in "EasyTest" cell. Int J Hydrogen Energy 2007;32:872–7.

[4] Radev I, Georgiev G, Sinigersky V, Slavcheva E. Proton conductivity measurements of PEM performed in easy test cell. Int J Hydrogen Energy 2008;33:4849–55.

[5] Kim KH, Kim HJ, Lee KY, Jang JH, Lee SY, Cho E, et al. Effect of Nafion® gradient in dual catalyst layer on proton exchange membrane fuel cell performance. Int J Hydrogen Energy 2008;33:2783–9.

[6] Kita H. Periodic variation of exchange current density of hydrogen electrode with atomic number and reaction mechanism. J Electrochem Soc 1966;113:1095–111.

[7] Lee K, Zhang J, Wang H, Wilinson DP. Progress in the synthesis of carbon nanotube- and nanofiber-supported Pt electrocatalysts for PEM fuel cell catalysis. J Appl Electrochem 2006;36:507–22.

[8] Trasatti S. Electrocatalysis in the anodic evolution of oxygen and chlorine. Electrochim Acta 1984;29:1503–12.

[9] Jakšić MM. Advances in electrocatalysis for hydrogen evolution in the light of the Brewer-Engel valence-bond theory. Int J Hydrogen Energy 1987;12:727–52.

[10] Jakšić MM. Brewer intermetallic phases as synergetic electrocatalysts for hydrogen evolution. Mater Chem Phys 1989;22:1–26.

[11] Neophytides SG, Zafeiratos S, Papakonstantinou GD, Jakšić JM, Paloukis FE, Jakšić MM. Extended Brewer hypo–hyper-d-interionic bonding theory – I. Theoretical considerations and examples for its experimental confirmation. Int J Hydrogen Energy 2005;30:131–47.

[12] Paunović P. Mixed nano-scaled electrode materials for hydrogen evolution. In: Reithmaier JP, Petkov P, Kulish W, Popov C, editors. Nanostructured materials for advanced technological applications. Springer Science + Business Media B.V; 2009. p. 391–8.

[13] Tauster SJ, Fung SC, Garten RL. Strong metal-support interactions. Group 8 noble metals supported on titanium dioxide. J Am Chem Soc 1978;100:170–5.

[14] Serp P, Corrias M, Kalck P. Carbon nanotubes and nanofibers in catalysis. Appl Catal A Gen 2003;253:337–58.

[15] Sahaym U, Norton MG. Advances in the application of nanotechnology in enabling a 'hydrogen economy'. J Mater Sci 2008;43:5395–429.

[16] Paunović P, Dimitrov AT, Popovski O, Slavkov D, Hadži Jordanov S. Use of multiwalled carbon nanotubes (MWCNTS) as a support material in complex electrocatalysts for hydrogen evolution. Maced J Chem Chem Eng 2007;26:87–93.

[17] Paunović P, Dimitrov AT, Popovski O, Slavcheva E, Grozdanov A, Lefterova E, et al. Effect of activation/purification of multiwalled carbon nanotubes (MWCNTs) on activity of non-platinum based hypo–hyper d-electrocatalysts for hydrogen evolution. Mat Res Bull 2009;44:1816–21.

[18] Maillard F, Simonov PA, Savinova ER. Carbon materials as supports for fuel cell electrocatalysts. In: Serp P, Figueiredo JL, editors. Carbon materials for catalysis. New Jersey: John Wiley & Sons; 2009. p. 429–80.

[19] Paunović P, Popovski O, Dimitrov AT, Slavkov D, Lefterova E, Hadži Jordanov S. Improvement of performances of complex non-platinum electrode materials for hydrogen evolution. Electrochim Acta 2006;52:1810–7.

[20] Paunović P, Popovski O, Dimitrov AT, Slavkov D, Lefterova E, Hadži Jordanov S. Study of structural and electrochemical characteristics of Co-based hypo–hyper d-electrocatalysts for hydrogen evolution. Electrochim Acta 2007;52:4640–8.

[21] Paunović P, Popovski O, Hadži Jordanov S, Dimitrov A, Slavkov D. Modification for improvement of catalysts materials for hydrogen evolution. J Serb Chem Soc 2006;71:149–65.

[22] Paunović P, Popovski O, Radev I. Investigation of cell assemblies prepared out of electrocatalysts aimed for hydrogen evolution. Bull Chem Technol Macedonia 2005;24(2):133–41.

[23] Paunović P, Radev I, Dimitrov AT, Popovski O, Lefterova E, Slavcheva E, et al. New nano-structured and interactive supported composite electrocatalysts for hydrogen evolution with partially replaced platinum loading. Int J Hydrogen Energy 2009;34:2866–73.

[24] H-J Kim, H-D Kim. 'Fitt' program for XPS curve analysis, http://escalab.snu.ac.kr/~berd/Fitt/fitt.html, accessed July 2008.

[25] Stoyanova AE, Lefterova ED, Nikolova VI, Iliev PT, Dragieva ID, Slavcheva EP. Water splitting in PEM electrolysis with Ebonex supported catalysts. Bulg Chem Commun 2010;42:167–73.

[26] Soin N, Roy SS, Karlsson L, McLaughlin JA. Sputter deposition of highly dispersed platinum nanoparticles on carbon nanotube arrays for fuel cell electrode material. Diam Relat Mater 2010;19:595–8.

[27] Utsumi S, Honda H, Hattori Y, Kanoh H, Takahashi K, Sakai H, et al. Direct evidence on C–C single bonding in single-wall carbon nanohorn aggregates. J Phys Chem C 2007;111:5572–5.

[28] Jung A, Graupner R, Ley L, Hirsch A. Quantitative determination of oxidative defects on single walled carbon nanotubes. Phys Stat Sol (b) 2006;243:3217–20.

[29] Vericat C, Wakisaka M, Haasch R, Bagus PS, Wieckowsk A. Binding energy of ruthenium submonolayers deposited on a Pt(111) electrode. J Solid State Electrochem 2004;8:794–803.

[30] Rizzi GA, Magrin A, Granozzi G. Substitutional $Ti_{(1-x)}Ru_xO_2$ surface alloys obtained from the decomposition of $Ru_3(CO)_{12}$ on TiO_2(110). Phys Chem Chem Phys 1999;1:709–11.

[31] Osman JR, Crayston JA, Pratt A, Richens DT. $RuO_2–TiO_2$ mixed oxides prepared from the hydrolysis of the metal alkoxides. Mater Chem Phys 2008;110:256–62.

[32] Kim J-G, Pugmire DL, Battaglia D, Langell MA. Analysis of the $NiCo_2O_4$ spinel surface with Auger and X-ray photoelectron spectroscopy. Appl Surf Sci 2000;165:70–84.

[33] Briggs D, Gibson VA. Direct observation of multiplet splitting in 2P photoelectron peaks of cobalt complexes. Chem Phys Lett 1974;25:493–6.
[34] Mekki A, Holland D, Ziq K, McConville CF. XPS and magnetization studies of cobalt sodium silicate glasses. J Non-Cryst Solids 1997;220:267–79.
[35] Kocijan A, Milošev I, Pihlar B. Cobalt-based alloys for orthopaedic applications studied by electrochemical and XPS analysis. J Mater Sci Mater Med 2004;15:643–50.
[36] Todorova S, Kolev H, Holgado JP, Kadinov G, Bonev C, Pereñíguez R, et al. Complete n-hexane oxidation over supported Mn–Co catalysts. Appl Catal B Environ 2010; 94:46–54.
[37] Shukla AK, Neergat M, Bera P, Jayaram V, Hegde MS. An XPS study on binary and ternary alloys of transition metals with platinized carbon and its bearing upon oxygen electroreduction in direct methanol fuel cells. J Electroanal Chem 2001;504:111–9.
[38] Aricò AS, Cretì P, Antonucci PL, Cho J, Kim H, Antonucci V. Optimization of operating parameters of a direct methanol fuel cell and physico-chemical investigation of catalyst–electrolyte interface. Electrochim Acta 1998;43:3719–29.
[39] Sato N, Ohtsuka T. Anodic oxidation of cobalt in neutral and basic solution. J Electrochem Soc 1978;125:1735–40.
[40] Burke LD, Murphy OJ. Electrochromic behaviour of oxide films grown on cobalt and manganese in base. J Electroanal Chem 1980;109:373–7.
[41] Hadži Jordanov S. Towards the year 2000: some aspects of the electrochemistry in the last decades of twentieth century. Bull Chem Technol Macedonia 1997;16:75–88.
[42] Boodts JCF, Trsatti S. Hydrogen evolution on iridium oxide cathodes. J Appl Electrochem 1989;19:255–62.